

ISO-SWS observations of infrared absorption bands of the diffuse interstellar medium: The 6.2 μm feature of aromatic compounds^{*}

W.A. Schutte¹, K.A. van der Hucht², D.C.B. Whittet³, A.C.A. Boogert⁴, A.G.G.M. Tielens⁴, P.W. Morris⁵, J.M. Greenberg¹, P.M. Williams⁶, E.F. van Dishoeck¹, J.E. Chiar⁷, and Th. de Graauw⁸

¹ Leiden Observatory, P.O. Box 9513, 2300 RA Leiden, The Netherlands

² Space Research Organization Netherlands, Sorbonnelaan 2, 3584 CA Utrecht, The Netherlands

³ Department of Physics, Applied Physics and Astronomy, Rensselaer Polytechnic Institute, Troy, NY 12180, USA

⁴ Kapteyn Astronomical Institute, P.O. Box 800, 9700 AV Groningen, The Netherlands

⁵ ISO Science Operations Centre, ESA Astrophysics Division, VILSPA, P.O. Box 50727, E-28080 Madrid, Spain

⁶ Royal Observatory, Blackford Hill, Edinburgh EH9 3HJ, UK

⁷ NASA-Ames Research Center, MS 245-3, Moffett Field, CA 94035, USA

⁸ Space Research Organization Netherlands, P.O. Box 800, 9700 AV Groningen, The Netherlands

Received 19 August 1997 / Accepted 3 June 1998

Abstract. We present ISO-SWS spectroscopy of eight strong infrared sources with large extinction through the diffuse interstellar medium. These are five late-type Wolf-Rayet stars, the blue hypergiant Cyg OB2 #12 and the Galactic Center Sources 3 and 4. The spectra show a number of absorption features that can be ascribed to interstellar dust and gas. Features at 3.0, 3.4, 4.66 and 5.95 μm were already known from ground and airborne observations, while features at 4.27 and 6.21 μm are for the first time observed by ISO. We ascribe the 3.0, 4.27 and 4.66 μm features to H₂O ice, CO₂ ice and gaseous CO, respectively, located in dense clouds along four lines-of-sight in our study. Based on an excellent correspondence with the well-known emission feature observed in many other objects, the 6.2 μm absorption band is identified with aromatic materials. The profile of the feature indicates that its carriers are PAHs or PAH clusters containing up to a few thousand carbon atoms. The lack of strong infrared features of hydroxy (OH), carbonyl (C=O) and aromatic CH groups towards the objects of the present study shows that the carbonaceous dust material in the diffuse ISM is poor in oxygen as well as hydrogen.

Key words: infrared: ISM: lines and bands – Galaxy: abundances – ISM: dust, extinction – methods: observational

1. Introduction

The term “diffuse interstellar medium” denotes the vast, very low density regions which account for the bulk of the volume of our Galaxy. Here densities range from $\sim 10^{-3}$ H atoms cm^{-3}

for the hot intercloud gas up to a few hundred H atoms cm^{-3} for diffuse molecular clouds (Jura 1987). Chemically the diffuse medium is characterized by a low content of molecular gas; i.e., while H₂ can account for up to $\sim 50\%$ of the hydrogen in diffuse molecular clouds, this fraction is much less in most lines-of-sight (van Dishoeck & Black 1986; Meyer 1997). The fraction of CO is lower than 5×10^{-6} relative to hydrogen even for relatively dense diffuse regions (van Dishoeck & Black 1986). Theoretical calculations indicate that refractory dust particles (silicate, graphite, amorphous carbon) can survive the harsh conditions of these environments considerably better than frozen volatiles (Jones et al. 1994; 1996), consistent with the absence of infrared absorption bands due to ices in diffuse lines-of-sight (e.g., towards Cyg OB2 #12; Gillett et al. 1975; Pendleton et al. 1994).

Many aspects of the nature of the dust in the diffuse galactic medium are still unclear. While the strong and broad Si-O stretch interstellar absorption feature at 9.7 μm clearly shows the presence of amorphous silicates, the optical properties of silicates and the abundance of Si preclude these materials as the sole carrier of the visual extinction (Spitzer 1978; Greenberg 1974). Therefore an additional component needs to be invoked. Based on cosmic abundance considerations as well as durability under the harsh environment of diffuse galactic space, it is generally assumed that the missing dust should be carbonaceous in nature. Moreover, the strong bump in the interstellar extinction curve at 217 nm is generally ascribed to carbonaceous solids (e.g., Draine 1989; Mennella et al. 1996; Schnaiter et al. 1998). Various models using a combination of carbonaceous and silicate dust (either as separate particles, or as particles consisting of a silicate core with carbonaceous mantle) succeed in fitting the interstellar extinction curve (e.g., Kim et al. 1994; Mathis 1996; Li & Greenberg 1997). No matter what forms of carbonaceous dust are assumed (graphite, Hydrogenated Amorphous Carbon (HAC) particles, Organic Refractory (OR) mantles on silicate

Send offprint requests to: W.A. Schutte

^{*} Based on observations with ISO, an ESA project with instruments funded by ESA Member States (especially the PI countries: France, Germany, the Netherlands and the United Kingdom) and with the participation of ISAS and NASA.

particles), these models agree that the fraction of carbon in dust must be substantial ($> 50\%$ of the cosmic abundance). Ground-based and airborne infrared spectroscopy of sources towards the galactic center and more local obscured objects indeed reveals two absorption features of carbonaceous solids; i.e., the aliphatic CH stretching and bending modes at 3.4 μm and 6.8 μm (Wickramasinghe & Allen 1980; Butchart et al. 1986; Sandford et al. 1991; Pendleton et al. 1994; Tielens et al. 1996; Imanishi et al. 1996). Airborne spectroscopy also gives tentative indications for the presence of features due to organic carbonyl groups (Tielens et al. 1996). However, the total amount of carbon involved in these features falls well short of the quantity needed to explain the interstellar extinction. Thus it has been generally assumed that the bulk of the carbonaceous dust in the diffuse interstellar medium has at most weak infrared absorption bands, e.g., amorphous aromatic or even diamond-like material with little oxygen, nitrogen or hydrogen.

Recent results from the Infrared Space Observatory (ISO) and Infrared Telescope in Space (IRTS) have shown that the well known “unidentified” infrared emission (UIR) bands at 6.2, 7.7, 8.6 and 11.3 μm are ubiquitously present in the diffuse galactic emission (Lutz et al. 1996; Onaka et al. 1996). These bands are generally attributed to gas phase Polycyclic Aromatic Hydrocarbon (PAH) molecules and small PAH clusters (Léger & Puget 1984, Allamandola et al. 1985). These results show that besides refractory dusts, the diffuse medium also contains an important molecular component. The intensity of the features indicate that the PAHs are quite abundant, although they probably contain less carbon than the dust (Dwek et al. 1997).

The Infrared Space Observatory (ISO; Kessler et al. 1996) for the first time provides a complete view of the mid-infrared spectral region from 2.5 to 20 μm ($4000\text{--}500\text{ cm}^{-1}$) by means of the Short Wavelength Spectrometer (SWS; de Graauw et al. 1996a). This paper reviews such observations towards a number of luminous sources which are highly obscured by diffuse medium dust, thus providing a sensitive search for weak dust absorption features. These are five Wolf-Rayet stars; i.e., WR118 (GL2179), WR112 (GL2104), WR104 (Ve2-45), WR98a (IRAS 17380-3031) and WR48a, and additionally Cyg OB2 #12 (VI Cyg #12) and the Galactic Center Sources GCS 3 and GCS 4. Earlier reports of these spectra were given by van der Hucht et al. (1996) for the WR stars and by Whittet et al. (1997) for Cyg OB2 #12.

The paper is laid out as follows. Sect. 2 discusses the nature of the sources. In Sect. 3 observational aspects are reviewed. Sect. 4 summarizes and identifies the detected absorption features. Sect. 5 considers whether the detected 6.2 μm absorption band originates in gaseous or dust material. Sect. 6 reviews the constraints on the chemical composition of the carbonaceous dust material in the diffuse medium set by the present observations. In Sect. 7 the implications of our results for the condition of gaseous and solid carbonaceous material in dense and diffuse clouds are discussed. Finally, Sect. 8 summarizes the conclusions of this paper.

2. Nature of the sources

The objects WR118, WR112, WR104, WR98a, and WR48a are Population I, C-rich Wolf-Rayet stars. These stars drive a high mass-loss rate, forming hot carbonaceous dust in their stellar winds (cf. Williams 1995; van der Hucht 1992). The hot dust provides a strong source of infrared continuum emission, making these sources excellent probes of foreground absorption features of interstellar origin.

Cyg OB2 #12 is a highly luminous star of spectral type B5Ia⁺ (Humphreys 1978). No dust appears to be associated with the star, and the mid-infrared emission can be attributed entirely to the hot photosphere combined with the radiation produced by free-free and free-bound transitions of ionized hydrogen in the strong stellar wind (Persi & Ferrari-Toniolo 1982; Leatherer et al. 1984). For this reason the infrared spectrum has a relatively blue slope, making Cyg OB2 #12 a less sensitive probe than the WR stars for absorption bands longward of $\sim 5\ \mu\text{m}$.

The Galactic Center sources GCS 3 and GCS 4 make up the so-called infrared quintuplet located near the “radio arc” prominent in radio maps of the galactic center region (Okuda et al. 1990; Nagata et al. 1990). These sources are also known as GL 2004. GCS 3 consists of 4 separate sources concentrated in a region of 9" diameter. The SWS was centered on source GCS 3 II, the brightest component, but all four components are in the beam. The position of GCS 4 is 14" away from this source, and in view of the SWS aperture of 14" \times 20" (de Graauw et al. 1996a) traces an independent line-of-sight. The nature of the quintuplet sources is unclear. There is no sign of photospheric CO or H₂O or circumstellar maser emission, expected for late type giants or supergiants (Okuda et al. 1990; Nagata et al. 1990). The spectral energy distribution is however characteristic of warm (600 K) circumstellar dust. Their sky position (15' from the Galactic Center) and infrared polarization place these objects in the central region of our Galaxy (Nagata et al. 1990. Okuda et al. 1990). The derived luminosities range from 2.2×10^4 to $1.4 \times 10^5 L_{\odot}$ compatible with a cluster of embedded massive YSO's. However, there is no sign of Br γ , sometimes seen in such objects, and no evidence for a bipolar outflow. Various estimates agree on a visual extinction of 20–25 mag, comparable to that for the cluster in the Galactic Center (Okuda et al. 1990).

3. Observations

All observations were made with the ISO Short Wavelength Spectrometer (ISO-SWS). Full 2–45 μm spectra were obtained for all sources, with scanner speeds 2 or 3, resulting in resolving powers $R \sim 250$ and $R \sim 400$ respectively (‘AOT01’). Spectra at the full grating resolution ($R \sim 1500$) were also obtained around 6.2 μm for GCS 3 and Cyg OB2 #12 (‘AOT06’). Table 1 gives a summary of the observations.

The spectra were reduced within the SWS Interactive Analysis package. The “Standard Processed Data” files were derived with version 5.0 of the SWS pipeline for the AOT01 spectra, and version 6.1 for the AOT06 spectra. The reduction of the

Table 1. Observation log

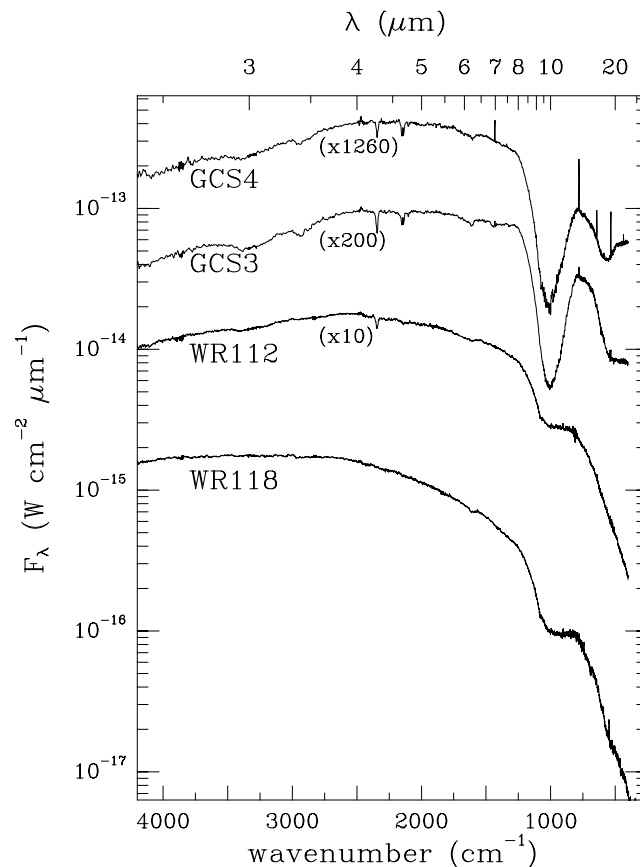
Object	Alt. name	Rev.	AOT	sp.	t_{int}
GCS 3		287	1	3	60 m
		327	6	–	52 m
GCS 4		297	1	3	60 m
Cyg OB2 #12	VI Cyg #12	682	6	–	25 m
WR48a	Danks 1	79	1	2	30 m
WR98a	IRAS17380	94	1	2	30 m
WR104	Ve2-45	99	1	2	30 m
WR112	GL2104	102	1	2	30 m
WR118	GL2179	108	1	2	30 m

Table 2. Observed absorption features and their assignments

cm^{-1}	Position μm	FWHM cm^{-1}	Assignment
3300	3.03	320	OH stretch ^a
2920	3.42	65	aliphatic CH stretch
2344	4.266	14	CO ₂ (solid)
2147	4.658	28	CO (gas)
1680	5.95	~ 100	Carbonyl CO stretch
1608–1618	6.18–6.22	35	aromatic CC stretch

^a Probably primarily due to solid H₂O (see text)

AOT01 spectra to the “Auto Analysis Result” was done with the calibration files available in May 1997. A small (1–5%) correction to the overall shape of the spectrum, and to some spurious features, was made in March 1998 with improved Relative Spectral Response Functions (RSRF) of SWS bands 2B and 2C (5.3–12.0 μm). The AOT06 spectra were reduced with the calibration files available in January 1998, also including the new RSRF’s. Each detector of all spectra was inspected for detector jumps and excessive noise levels. In the wavelength range relevant for this study (2.3–12.0 μm) only few detectors were affected by these problems, and affected wavelength regions were removed. Systematic differences in the flux scale and slope of the 24 detector up and down scans in each SWS detector band were corrected for by fitting straight lines to each scan and using these fits to shift the data points to a carefully selected reference spectrum. This reference spectrum was constructed from the data itself, leaving out scans with clearly deviating slopes and flux levels. The systematic differences between the scans are most likely caused by dark current variations due to detector memory effects, especially at wavelengths above 4 μm . Thereafter, data points affected by cosmic ray hits, deviating more than 2.7 sigma from the mean of all points per resolution element, were removed. Finally, the up and down scans were rebinned to a wavelength grid with $R = \lambda/\Delta\lambda = 250, 400,$ or 1500 (depending on the observing mode) and 2 points per resolution element, using the trapezoidal rule integration method. Small differences in flux level ($\leq 10\%$) at the band edges were corrected for by multiplication. To inspect the reliability of the final spectrum, the up and down scans were separately rebinned

**Fig. 1.** SWS spectroscopy of GCS 3, GCS 4, WR118 and WR112. For clarity, flux levels were multiplied by the indicated factor in some cases

and compared. A very good agreement was found for the continuum and broad dust features. On a smaller scale, systematic differences between the scans determine the effective signal-to-noise. At 6.0 μm the AOT01’s thus have a signal-to-noise of ~ 50 , while for the AOT06 spectra a value of ~ 85 is obtained.

We note that at the current stage of development of the reduction package weak ($\tau \leq 0.04$), broad (FWHM $\geq 60 \text{ cm}^{-1}$) features may still be susceptible to uncertainties in the adopted RSRF function.

4. The interstellar absorption features

Fig. 1 shows the 4200–250 cm^{-1} (2.4–40 μm) spectra of WR112, WR118, GCS 3 and GCS 4. To highlight the weaker interstellar bands, we display the same spectra up to the onset of the strong 9.7 μm silicate feature in Fig. 2. No features besides the 9.7 and 18.5 μm silicate bands are seen longward of 8.3 μm . Table 2 lists all mid-infrared absorption bands that were found in this spectral region for the eight sources of this study, together with their assignments (see below). Some sources, e.g., GCS 3, show all features while others, such as WR118, show only the 3.4 μm and 6.2 μm bands.

While the 3.0 μm O–H stretching mode, the 3.4 μm C–H stretching mode and the 4.66 μm feature of gaseous CO have already been observed from the ground (Pendleton et al. 1994;

Table 3. Integrated optical depth τ_{int} (Eq. 1) and/or peak depth τ of the interstellar absorption bands, and visual extinction towards the various sources. For band positions and widths, see Table 2

	WR118	WR112	WR104	WR98a	WR48a	Cyg OB2	GCS 3	GCS 4
$\tau_{\text{int}}(\text{OH str.}) (\text{cm}^{-1})$	< 17	34 \pm 8	< 14	17 \pm 8	< 10	< 11	120 \pm 20	80 \pm 20
$\tau(\text{OH str.}) (\times 100)$	< 5	8 \pm 4	< 2	< 4	< 3	< 3	38 \pm 6	25 \pm 6
$\tau(\text{aliph. CH str.})^{\text{a}} (\times 100)$	5.2	4.4	2	–	–	4.6	13 \pm 1	10 \pm 2
$\tau_{\text{int}}(\text{CO}_2) (\text{cm}^{-1})$	< 0.4	3.1	< 0.3	0.8	< 1.6	< 1	5.4	3.7
$\tau(\text{CO}_2) (\times 100)$	< 2.5	17	< 2	4	< 9	< 6	34	25
$\tau_{\text{int}}(\text{CO}_{\text{gas}}) (\text{cm}^{-1})$	< 1.2	1.8	< 0.5	0.3	< 2	< 1.5	6.9	4.6
$\tau_{\text{int}}(\text{arom. CC str.}) (\text{cm}^{-1})$	2.2 \pm 0.6	1.3 \pm 0.6	0.6 \pm 0.3	1.5 \pm 1	0.6 \pm 0.5	\leq 1.1	4.7 \pm 0.6	3.1 \pm 1.0
$\tau(\text{arom. CC str.}) (\times 100)$	6.0 \pm 2.0	4.0 \pm 2.0	1.7 \pm 0.9	4.3 \pm 3.0	1.7 \pm 1.5	\leq 2.5	13 \pm 3	9 \pm 3
$\tau_{\text{int}}(\text{Carb. CO str.}) (\text{cm}^{-1})$	1.6 \pm 0.8	3.3 \pm 1.5	3.0 \pm 1.2	1.5 \pm 1.0	3.3 \pm 1.7	\leq 1.8	3.7 \pm 1.2	3.1 \pm 1.2
$\tau(9.7)$	0.71	0.56	0.30	0.64	0.52	0.54 ^b	2.4	2.2
$\frac{\tau_{\text{int}}(\text{CCstr.})}{\tau(9.7)}$	3.1 \pm 1.1	2.3 \pm 0.9	2.0 \pm 1.1	2.3 \pm 1.6	1.2 \pm 1.0	\leq 2.0	2.0 \pm 0.3	1.4 \pm 0.5
$\frac{\tau(\text{CHstr.})}{\tau(9.7)}$	2.4 \pm 0.9	3.4 \pm 1.5	3.3 \pm 1.7	–	–	\geq 4.2	2.8 \pm 0.4	3.2 \pm 1.1
$\frac{\tau_{\text{int}}(\text{CCstr.})}{\tau(\text{CHstr.})} (\times 100)$	0.073	0.079	0.067	–	–	0.085	0.054	0.046
A_{V}^{c}	12.8	12.0	6.5	11.2	7.7	10.2	23 \pm 2	23 \pm 2
$\frac{A_{\text{V}}}{\tau(9.7)}$	18.0	21.4	21.7	17.5	14.8	18.9	9.6	10.5

^a From ground-based observations (Pendleton et al. 1994), except for the GC sources;

^b From Whittet et al. (1997)

^c A_{V} from van der Hucht et al. (1996) for the WR stars, from Whittet et al. (1997) for Cyg OB2 #12 and from Okuda et al. (1990) for GCS 3 and GCS 4

Sandford et al. 1991; Okuda et al. 1990; Lacy et al. 1984), the 4.27 μm feature of CO_2 (de Graauw et al. 1996b; Gürtler et al. 1996) and the 6.2 μm band are first observed by ISO.

Table 3 lists the integrated strengths and/or the peak depth of all the features. The integrated strength τ_{int} is obtained from

$$\tau_{\text{int}} = \int_{\text{feat.}} \tau(\nu) d\nu. \quad (1)$$

where the feature optical depth $\tau(\nu)$ is obtained relative to an appropriate baseline (see below). In general it is preferable to use integrated intensities rather than peak depth, since the former is less sensitive to the spectral noise. For the 3.4 μm band, the noise level of the SWS spectra was, except for the GC sources, too high to obtain a good measurement. In this case the peak depths from ground-based observations were adopted (Pendleton et al. 1994), insofar available. Baselines were defined in the $\log(F_{\lambda})$ vs wavenumber plane by a smooth polynomial fit of the continuum regions on each side of the various features. This yielded satisfactory fits in all cases. For the relatively narrow 3.4 and 6.2 μm bands first order polynomials could produce good fits, while for the broad OH stretching and silicate feature smooth second, third and fourth order polynomials were applied. Our derived silicate band depths agree within 10% with earlier determinations which used a more thorough treatment of the continuum definition (Roche & Aitken 1984). To derive the integrated strength of the 6.2 μm band of GCS 3, GCS 4, and WR112, a correction was made for the overlapping OH bending mode of H_2O ice, which appears to be present towards these sources (see Sect. 4.4).

There is some indication of a shallow feature near 6.9 μm in the spectrum of GCS3, though not in any of the other spectra.

A similar feature has been seen towards Sgr A* (Tielens et al. 1996; Lutz et al. 1996). However, the quality of the present data is insufficient to insure the reality of this band (Sect. 3). For a detailed discussion of the 6.9 μm band we refer to Chiar et al. (in prep.).

Whittet et al. (1997) reported the detection of a weak feature near 2.75 μm (3640 cm^{-1}) towards Cyg OB2 #12 which was ascribed to the OH^- ion inside the lattice of the amorphous silicate dust. No sign of this feature was found in any of the WR stars (e.g., Fig. 2). However, upper limits for the band depth are typically $\tau(2.75) < 0.04$, still consistent with the optical depth of 0.035 towards Cyg OB2 #12. Due to blending with the strong 3.0 μm feature, no significant upper limits to this feature can be set for GCS 3 and GCS 4.

4.1. Comparison with earlier observations

Earlier medium resolution ($\lambda/\Delta\lambda \approx 300$) airborne spectroscopy in the direction of the Galactic Center appeared to show absorption features near 5.8 and 5.5 μm (1720 and 1820 cm^{-1}), which were ascribed to the CO stretching mode of carbonyl groups (Tielens et al. 1996). The present data show no sign of the 5.5 μm feature towards GCS 3 and 4. This may be due to differences in the composition of the dust in these slightly different lines-of-sight; i.e., the quintuplet sources are 15' away from the Galactic Center. However, recent SWS observations of Sgr A* also show no sign of the 5.5 μm band (Lutz et al. 1996). On the other hand, the band near 5.95 μm , forming a shoulder on the blue side of the 6.2 μm band in all our sources, is very similar to the earlier reported 5.8 μm band.

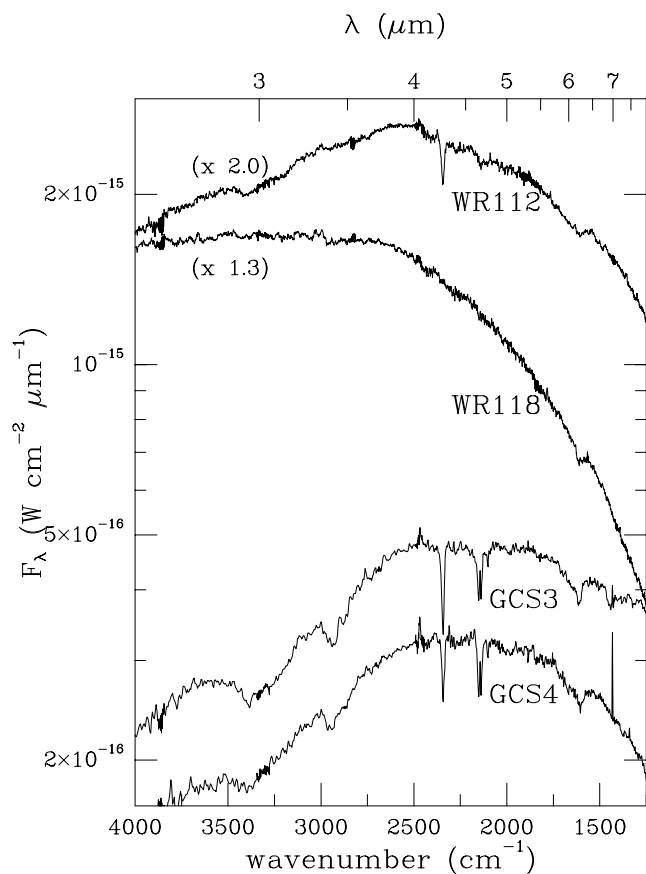


Fig. 2. As Fig. 1, enlarging the salient 4000–1250 cm^{-1} region

Airborne spectroscopy was previously obtained for WR112 (GL2104) and WR104 (Ve2-45) (Cohen et al. 1989). The 22'' aperture of these observations is quite compatible with the ISO-SWS beam. The spectra showed a broad absorption band near 6.0 μm (1670 cm^{-1}) and a broad emission feature at 7.8 μm (1280 cm^{-1}). No evidence for either of these features is apparent in the present data (Fig. 2). While at the earlier reported intensity the strong emission band should be clearly visible, perhaps the broad and shallow absorption feature is difficult to separate from the overall slope of the continuum and its presence may therefore depend on the choice of the (local) continua.

Ground-based IRTF spectra of WR112 (GL2104), WR118 (GL2179) and WR104 (Ve2-45) between 3550 and 2550 cm^{-1} (2.82–3.92 μm) were obtained by Pendleton et al. (1994). These data in general show good correspondence to the SWS AOT1 data with respect to overall slope and structure. Indeed, the IRTF data also show the shallow 3.0 μm feature towards WR112, while no sign of this band is present for the other two sources.

4.2. The 3.0, 4.27 and 4.66 μm features

The width (FWHM = 14 cm^{-1} ; 0.032 μm) and position (2344 cm^{-1} ; 4.266 μm) of the CO_2 band, as well as the absence of a double structure due to the P and the R branch of rovibrational transitions clearly imply an icy origin (de Graauw

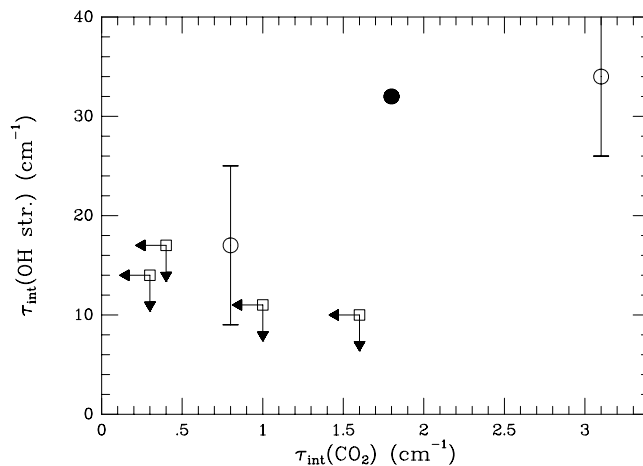


Fig. 3. The integrated optical depth of the solid CO_2 feature plotted against that of the OH stretching band. Open circles show actual detections, for squares only upper limits could be obtained for both the CO_2 and OH stretching features; cf. Table 3. For comparison, the filled circle shows the position of the protostellar object NGC7538:IRS9 (Whittet et al. 1996). The CO_2 and H_2O integrated band depths were both multiplied by 0.02 for this object

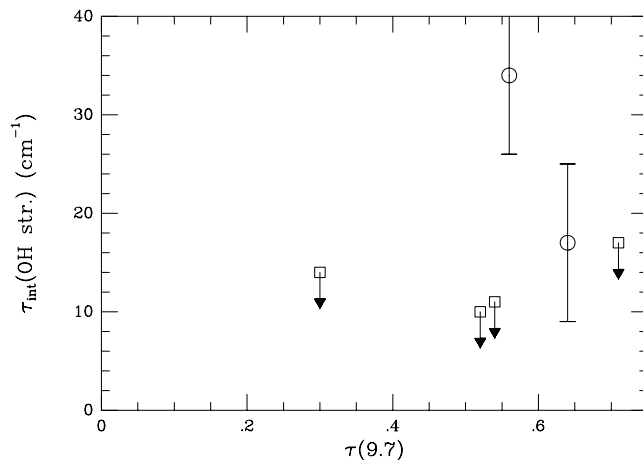


Fig. 4. The depth of the 9.7 μm silicate band plotted against the integrated optical depth of the OH stretching band. Circles show actual detections, for squares only upper limits could be obtained for the OH stretching feature; cf. Table 3

et al. 1996b; van Dishoeck et al. 1996). The presence of CO_2 ice indicates some dense cloud extinction towards four of our sources (Table 3). An additional feature is present at 2147 cm^{-1} (4.658 μm) for these same four objects, which can be ascribed to CO. Due to the low S/N level and resolution, rotational substructure cannot be distinguished, but the overall width and shape are very similar to the gas phase CO band seen towards Sgr A* (Lutz et al. 1996), while it is much broader than the solid state CO features seen towards embedded protostellar sources or background field stars (e.g., Tielens et al. 1991; Chiar et al. 1995). Indeed, for GCS 3 and GCS 4, high resolution ground-based data shows the presence of rotational levels in the P and R branches (Okuda et al. 1990). We thus conclude that the 4.66 μm feature

originates in gaseous CO. The CO band correlates well with the solid CO₂ feature (Table 3), indicating an origin in dense cloud material along the line-of-sight.

The origin of the 3.0 μm OH stretching band in diffuse lines-of-sight such as those in the present study has long been controversial. It has been ascribed to organic OH groups (Schutte & Greenberg 1986), to water of hydration embedded in silicates (Wada et al. 1991; Tielens et al. 1996), and to water ice located in some dense material intercepting the line-of-sight (Schutte & Greenberg 1988; McFadzean et al. 1989).

Figs. 3 and 4 plot the integrated optical depth of the OH feature against the CO₂ and silicate features, respectively, for the local sources. We did not include the two GC sources in these figures, since the long line-of-sight and high extinction towards these objects would tend to hide any (non-) correlations that may exist between independent dust components because of the many different environments that are probed. It can be seen from Fig. 3, as well as directly from the spectra (Fig. 2), that, in the limited set of available data, the OH feature is stronger for stronger CO₂ bands. Indeed, the OH band is exclusively present when the CO₂ feature is observed as well. There appears to be no correlation of the OH feature with the silicate band (Fig. 4; see also Whittet et al. 1997). These observations point to an origin of the OH stretching mode in dense material. In this case the feature should probably be primarily ascribed to H₂O ice. Fig. 3 shows that the ratio CO₂ to H₂O ice would then be slightly higher than what is found in a typical dense cloud source (NGC7538:IRS9; Whittet et al. 1996). In any case, the absence of any discernable OH band in lines-of-sight without CO₂ places stringent upper limits to the amount of H₂O of hydration or organic OH groups in the silicate and organic components of diffuse medium dust (Sect. 6).

We note that, while the CO₂, H₂O and CO gas features in the spectra of four of our sources indicates dense cloud material in the line of sight, the weakness of the 3 μm water feature shows that the fraction of dense extinction is small (cf., Whittet et al. 1988).

4.3. The 3.4 μm feature

The 3.4 μm feature has already been extensively observed from the ground for a large number of objects obscured by diffuse medium dust. It is ascribed to the aliphatic CH stretching mode of carbonaceous dust material (e.g., Pendleton et al. 1994; Greenberg et al. 1995). Matching this feature with various organic materials suggested that the aliphatic groups may be attached to aromatic structures (Pendleton et al. 1994).

4.4. The 6.2 μm feature

In contrast to the OH stretching band, the 6.2 μm feature shows no correlation with the CO₂ and CO features, but appears to be present in all lines-of-sight along with the aliphatic CH stretching band (Table 3, Fig. 2). We thus conclude that this feature is associated with the diffuse medium.

Figs. 5 to 7 show the 6.2 μm absorption feature in the various sources. Besides the relatively sharp 6.2 μm feature, the spectra also show the broad 5.95 μm feature, which will be discussed below. For GCS 3 and Cyg OB2 #12 the AOT6 data are plotted. All spectra were smoothed to resolution 4 cm^{-1} . WR48a is omitted because of its high noise level. To highlight the 6.2 μm and 5.95 μm features, we subtracted a linear baseline from the spectrum in the $\log(F_\lambda)$ vs wavenumber plane. The continuum ranges were selected around 1800 and 1400 cm^{-1} . We emphasize that this procedure does not in any way represent a “true” continuum subtraction, but should only be regarded as a cosmetic operation enabling a clearer view of the structure present in the 6 micron region. We prefer not to subtract any higher order polynomials to avoid loss of broad structure that could be present in the data.

Some overall curvature is present in the various spectra shown in Figs. 5 to 7. This can probably be attributed to the curvature of the continuum associated with the thermal dust emission from the various sources. There is no clear indication of the presence of emission bands. Various forms of solid carbon display features in this region, primarily ascribed to the CC stretching modes in aromatic moieties (Borghesi et al. 1987; Scott & Duley 1996; Scott et al. 1997; Schnaiter et al. 1998; Guillois et al. 1996). These structures could be emitted by the hot carbonaceous dust around the WR stars. However, only for WR104 there may be some indication of a broad emission feature centered at $\sim 6.3 \mu\text{m}$.

The GC sources, WR112 and WR98a show OH stretching 3 μm bands, presumably caused by H₂O ice (Sect. 4.2). In this case, the OH bending mode of H₂O should be present on the blue side of the 6.2 μm band. To indicate the expected strength of this feature, Figs. 5 to 7 show the H₂O feature of the ice mixture H₂O/CO/NH₃/O₂ = 0.32/0.23/0.13/0.32. This mixture was shown to give an excellent match to the 3 μm feature towards various Galactic Center infrared sources (Schutte & Greenberg 1988; Schutte 1988; Tielens et al. 1996). The feature was scaled according to the H₂O column density obtained from the 3 μm band.

Figs. 5 to 7 allow a comparison of the 6.2 μm feature in our objects to the (inverted) emission band of the planetary nebula NGC7027 (from Beintema et al. 1996). This spectrum represents the (average) CC stretching feature associated with emission by interstellar gaseous Polycyclic Aromatic Hydrocarbons (PAHs; Léger & Puget 1984; Allamandola et al. 1989). Furthermore, features of two laboratory materials are shown; i.e., the aromatic CC stretching mode in anthracite coal (Guillois et al. 1996), and the OH bending mode in H₂O of hydration in talc (From Tielens et al. 1996). Other cases of H₂O of hydration, such as hydrated SiO and trapped H₂O in the Murchison meteorite, give a similar broad band near 6.2 μm (FWHM = 60 - 100 cm^{-1} ; Wada et al. 1991). The coal feature represents the CC stretching modes of aromatic moieties in solid carbon. It falls slightly redward of the NGC7027 feature (at 1594 cm^{-1} vs. 1609 cm^{-1} for NGC 7027), and is considerably broader (60 vs 40 cm^{-1}). Other such materials, such as various forms of laboratory produced Hydrogenated Amorphous Carbon or

semi-anthracite coal, give a band of similar position and width (Borghesi et al. 1987; Guillois et al. 1996; Scott & Duley 1996; Scott et al. 1997; Schnaiter et al. 1998). Generally, the laboratory materials were thermally treated to get rid of oxygen and excess hydrogen which give rise to strong features near 5.8 and 6.9 μm .

H_2O of hydration has been proposed as a component of interstellar silicates (Tielens et al. 1996, van der Hucht et al. 1996). Comparison of Figs. 5 to 7 shows that the feature of H_2O of hydration is considerably broader than the observed absorption band. Moreover, the OH bending mode is accompanied by a broad OH stretching mode near 3 μm which is 20 times stronger (Tielens 1996; d'Hendecourt & Allamandola 1986). Although a broad 3 micron band is seen in a number of our objects, this feature is absent in other sources, while the 6.2 μm band is consistently present. E.g., towards WR 118, the 3 μm band is not seen, implying that its integrated optical depth is at most 10 times higher than that of the 6.2 μm feature (Table 3). Indeed the 3 μm feature appears to be associated with dense rather than the diffuse material in the line of sight (Sect. 4.2). We thus conclude that H_2O of hydration cannot be the carrier of the 6.2 μm band. Likewise, solid H_2O can be excluded as the carrier, since its OH bending mode is too blue and because of the weakness of the OH stretching feature near 3 μm , (d'Hendecourt & Allamandola 1986).

A close correspondence in position and width between the 6.2 μm absorption band and the emission feature of NGC 7027 is evident from considering Figs. 5 to 7. The emission feature is assigned to the CC stretching mode of gas phase Polycyclic Aromatic Hydrocarbons (PAHs; Léger & Puget 1984; Allamandola et al. 1989). Since the emission originates from excited PAHs, higher vibrational levels will contribute. This would cause a small red-shift (Joblin et al. 1995; Cook & Saykally 1998). At 450 K, the approximate temperature of peak emission in the 6.2 μm band, laboratory measurements give a shift of $\sim 15 \text{ cm}^{-1}$ (Cook & Saykally 1998), so that the ensemble of PAHs which emit the 6.2 μm band at 1609 cm^{-1} are expected to produce an absorption feature at $\sim 1624 \text{ cm}^{-1}$. This position is slightly to the blue of the absorption band (Table 1). However, the temperature shifts were measured for small neutral PAHs of 20–30 C atoms, while the PAHs emitting the 6.2 μm band are more likely to be ionized and to contain several hundreds of C atoms (Schutte et al. 1993). Therefore the exact magnitude of the temperature shift of the interstellar emitters is rather uncertain. We conclude that the close correspondence in position and width of the 6.2 μm emission and absorption features could suggest a similar origin.

While the emission feature must originate in gaseous PAHs due to excitation requirements, the absorption feature could also arise in carbonaceous solids with aromatic moieties, although the spectroscopic match, e.g., anthracite, appears less favorable in this case (see Figs. 5 to 7). The issue whether the carrier is solid or gaseous will be discussed in detail in Sect. 5.

In emission, a strong and very broad (FWHM = 0.6 μm / 100 cm^{-1} ; Beintema et al. 1996) band centered at $\sim 7.8 \mu\text{m}$ (1280 cm^{-1}) always accompanies the 6.2 μm feature (Russell

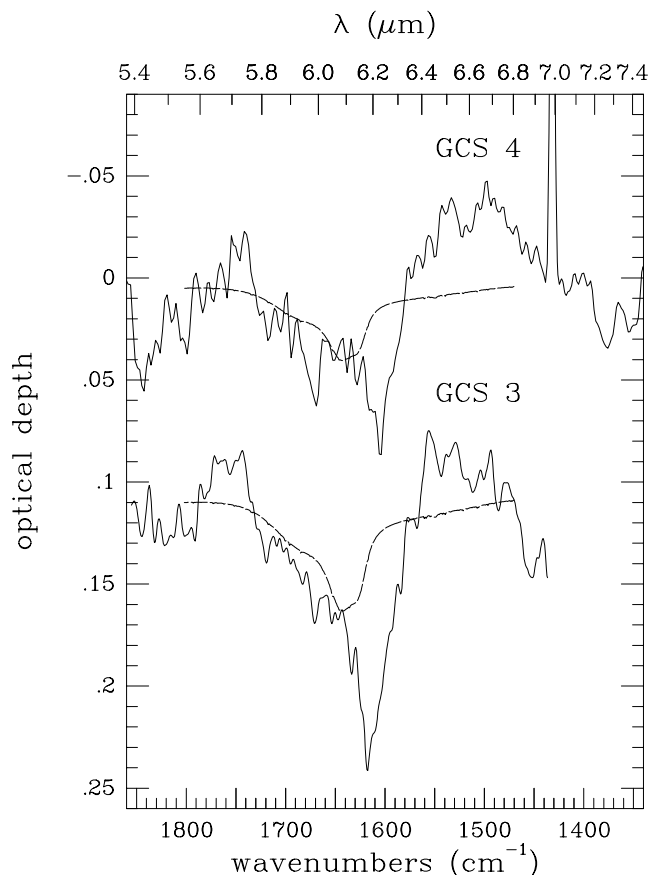


Fig. 5. The 6.2 μm absorption feature towards GCS 3 and GCS 4. The dashed curves indicate the expected contribution of the OH bending mode of solid H_2O expected to be present for sources which show the 3 μm absorption band. For clarity, arbitrary offsets are used

et al. 1977; Willner et al. 1977; Bregman et al. 1989; Cohen et al. 1986). In the diffuse galactic emission, the peak flux of this feature is ~ 1.5 times higher than the 6.2 μm emission band (Mattila et al. 1996; Onaka et al. 1996). This band, likewise due to aromatic CC stretching modes, should be present as well in absorption if the above identification is correct. However, this feature could be quite difficult to detect because it falls right on the edge of the onset of the very deep silicate feature. Fig. 8 searches for the 7.8 μm feature in the spectra of GCS3 and GCS4. These sources have the deepest 6.2 μm bands (Table 3) and are therefore most suitable to look for signs of the 7.8 μm feature. In Fig. 8 the inverted emission spectrum of NGC7027 (from Beintema et al. 1996) is subtracted from the GCS spectra to compensate for the 6.2 μm band. To take into account excitation effects, the intensity of the 7.8 μm band is decreased by 14% relative to the 6.2 μm band in the inverted NGC7027 spectrum. This adjustment is obtained from the standard PAH size distribution of Schutte et al. (1993) when comparing its absorption with its emission in a 10,000 K radiation field (see below). By making this subtraction, the baseline; i.e., the spectral shape without aromatic absorption bands, is restored if aromatic 6.2 & 7.8 μm absorption features are present. Indeed, for GCS4, this procedure appears to lead to a slight improvement in the

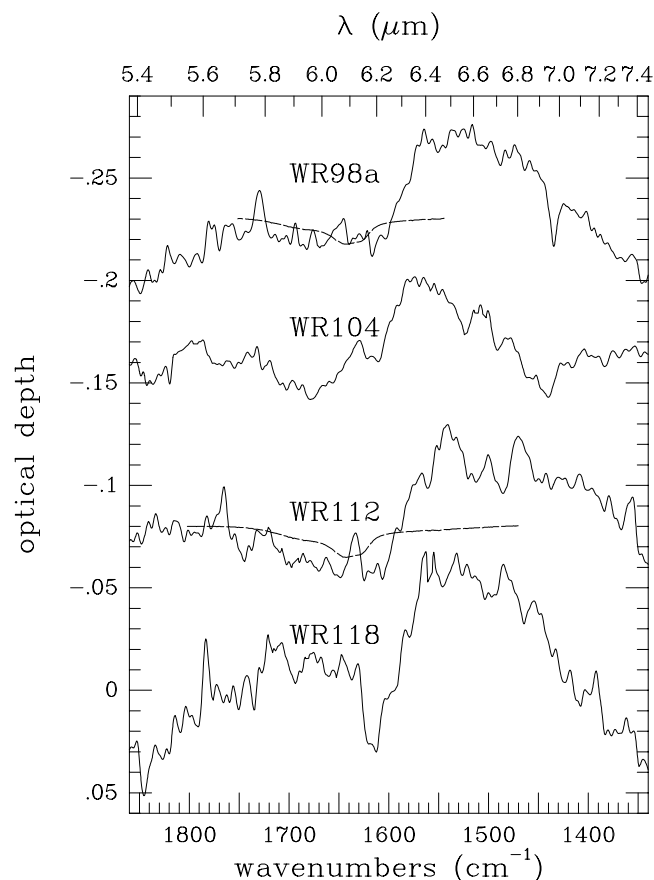


Fig. 6. As Fig. 5, but for the WR sources

“smoothness” of the baseline; i.e., the increase in the downward slope beyond $\sim 1500 \text{ cm}^{-1}$ is more gradual than that in the original data. For GCS3 adding the NGC7027 somewhat accentuates the shallow 6.9 μm absorption feature that seems to be present in this source, but again no baseline deviations are introduced. We conclude that the spectra of GCS3 and GCS4 are not inconsistent with the presence of a (hidden) 7.8 μm absorption feature.

No 11.24 μm (890 cm^{-1}) CH aromatic bending absorption feature is detected towards any of the objects of our study. The most significant upper limit is obtained towards WR118. Fig. 9 compares the relevant region of the spectrum with the (inverted) 11.2 μm emission band of NGC 7027. The upper limit equals $\tau_{int}(11.2) < 1.0 \text{ cm}^{-1}$; i.e., $\tau_{int}(11.2)/\tau_{int}(6.2) < 0.43$. For comparison, in emission the integrated intensities of the 6.2 and 11.2 μm features are similar (Mattila et al. 1996; Onaka et al. 1996). However, the relative intensities of the emission bands will be strongly influenced by excitation effects. The features are emitted by mostly ionized PAHs of size 30–500 C atoms. Such large ionized PAHs will absorb most energy in the visual region (Schutte et al. 1993, Salama & Allamandola 1993). In this region, the interstellar radiation field can be reasonably well represented by a diluted black body of temperature $\sim 10,000 \text{ K}$ (Spitzer 1978, Mathis et al. 1983). Under these conditions the “standard” interstellar PAH model of Schutte et al. (1993) pro-

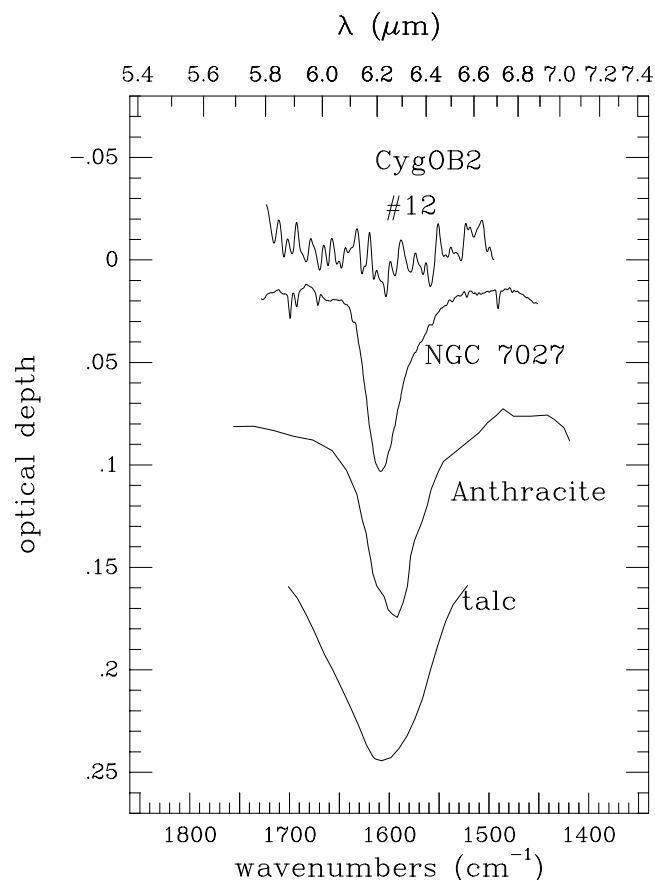


Fig. 7. Spectrum around 6.2 μm towards Cyg OB2 #12. For comparison are shown the emission band of the planetary nebula NGC 7027 (from Beintema et al. 1996, shown inverted), the 6.2 μm feature of the aromatic CC stretching mode in anthracite coal (Guillois et al. 1996), and the bending feature of water of hydration in talc (Tielens et al. 1996)

duces 2.1 times more flux in the 11.2 μm than 6.2 μm emission feature, somewhat larger than the emission ratio in the diffuse ISM. A straightforward analytical calculation yields, in absorption, for the same PAH ensemble an optical depth ratio 11.2/6.2 of only 0.39 (for a size distribution extending to 500 C atoms; i.e., the PAHs which emit their energy in the UIR bands rather than skeleton modes beyond $\sim 15 \mu\text{m}$). The reason for this difference is the strong enhancement of the 11.2 μm band in emission caused by the channelling of the flux into this band when a PAH during the relaxation phase which follows the absorption of a UV/Visual photon passes through the range 150–300 K. Here the 11.2 μm band is the main accessible emission channel, the temperature being too low for the 6.2 and 7.7 μm features to become significantly excited. In case of a solid state carrier, the low 11.2/6.2 ratio is consistent with the proposed assignment of the 6.2 μm band if the amount of hydrogen in this material is sufficiently low (see Sect. 6). We conclude that the present upper limit to the 11.2 μm absorption does not set strong constraints on the nature of the carrier of the 6.2 μm absorption. It is noted that if gaseous PAHs are the carrier of the band, a

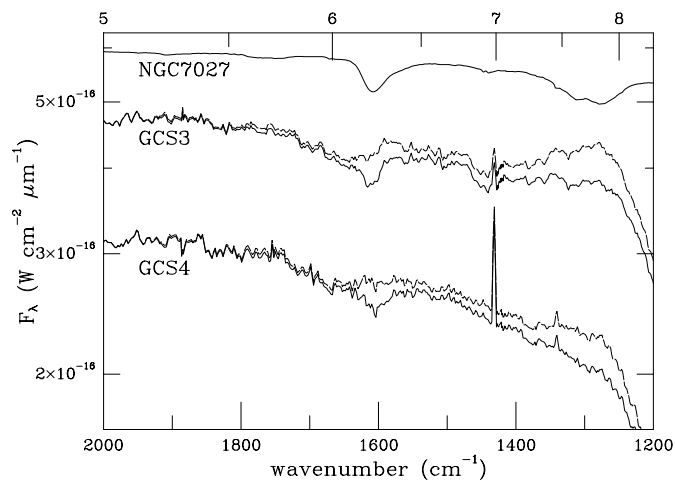


Fig. 8. Correction of the spectra of GCS3 and GCS4 for the aromatic absorption bands at 6.2 and 7.8 μm . The inverted NGC7027 PAH emission spectrum (from Beintema et al. 1996) is subtracted from both spectral curves eliminating the 6.2 μm feature. The NGC7027 spectrum has been slightly adjusted to take into account excitation effects (see text). Solid line: Original spectrum. Dashed line: After subtraction. A baseline was subtracted from the NGC7027 spectrum to correct for the continuum emission (Beintema et al. 1996), and furthermore sharp atomic and ionic lines were eliminated

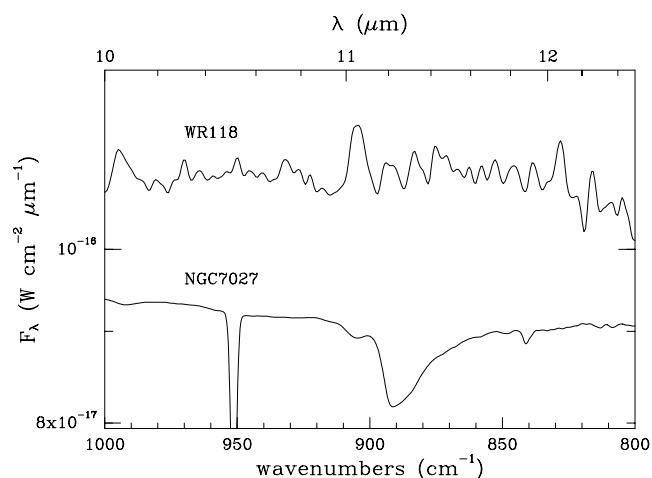


Fig. 9. A comparison between the spectra of WR118 and NGC7027 around the aromatic CH bending mode at 11.24 μm . The spectrum of NGC7027 has been inverted

modest improvement of the present S/N is expected to lead to a detection of the 11.2 μm absorption feature.

The aromatic CH stretching feature near 3.3 μm is not observed towards any of our objects. The intensity of the corresponding emission feature relative to the 6.2 μm feature in the diffuse galactic emission is about $I(3.3)/I(6.2) \approx 0.1$ (Ristorcelli et al. 1994). The most stringent upper limit to this feature (towards WR118) gives $\tau_{int}(3.3)/\tau_{int}(6.2) < 0.39$. Excitation effects should enhance the 3.3/6.2 ratio in absorption relative to emission, because only a limited section of the PAH size distribution can become sufficiently excited to emit in the 3.3 μm band. For the size distribution and spectroscopic properties of

the “standard” PAH model of Schutte et al. (1993), excited by a 10,000 K radiation field, an enhancement by a factor 2 is obtained. This indicates that the 3.3 μm absorption feature of the PAHs responsible for the diffuse UIR emission would fall below the present detection limit. In case of a solid state carrier the weakness of the 3.3 μm absorption band would confirm the low hydrogen content which is also indicated by the absence of the 11.2 μm feature (see Sect. 6). Thus, the absence of the 3.3 μm feature in the present data does not pose additional constraints on the nature of the carrier.

We conclude that the correspondence with the interstellar emission feature indicates that the 6.2 μm absorption and emission bands share a common origin; i.e., the CC stretching mode of aromatic materials.

In view of the carbonaceous dust shell surrounding the WR stars, a (partial) circumstellar origin of the 6.2 μm band needs to be considered for these objects. The visual extinction of the circumstellar material, as derived from the ratio of the stellar and circumstellar dust emission, is at most $A_V = 1$ (Williams et al., in prep.). This is only a small fraction of the total extinction for all our sources (Table 3). As will be discussed below, the observed integrated strength of the feature seems to imply that a substantial fraction of the total carbon in the line-of-sight needs to be involved in its carrier. Therefore if the dust would be homogeneously distributed in a circumstellar shell, it could at most account for only a small fraction of the absorption band. Indeed, for such a shell geometry, the 6.2 μm dust feature would show up in emission rather than in absorption (Williams et al., in prep.). However, possibly the circumstellar material could have a disk-type geometry and/or consist of optically thick clumps. In case of near edge-on viewing of a disk, the line-of-sight would become optically thick, resulting in a 6.2 μm absorption band. It is however unlikely that this situation would occur for all five WR stars of this study. On the other hand, if the outflow produces optically thick clumps of material, their infrared emission may display a 6.2 μm absorption band if there would be a sufficient temperature gradient across the clumps. We note however that both GC sources produce a 6.2 μm absorption feature of similar intensity relative to the interstellar 9.7 μm silicate band as the WR stars (Table 3). Neither of the GC sources is associated with circumstellar carbonaceous dust, so that in this case the feature should have an interstellar origin. Although Cyg OB2 #12 does not show a 6.2 μm absorption band, the derived upper limit is still consistent with a feature of intensity relative to the silicate band similar to the WR stars (Table 3). We conclude that the bulk of the 6.2 μm absorption feature in the WR stars should be of interstellar origin, but it cannot be excluded that there is a relatively small circumstellar contribution as well.

Summarizing, the 6.2 μm feature towards the WR stars and GC sources should originate in aromatic material (gas or solid) of (mainly) interstellar origin. We finally note that, while the 6.2 μm emission feature has been found in the diffuse galactic emission (Mattila et al. 1996), the intensity of this background emission is too weak to significantly decrease the strength of the absorption feature towards the bright infrared objects discussed here.

Table 4. Integrated strengths per C atom (A_C) of the 6.2 μm aromatic CC stretching mode in a number of molecules and bulk materials

Species	A_C cm/C	N_C/N_H^a
Neutral PAHs (average) ^d	2.0 (−19)	3.1 (−4)
PAH cations:		
Pyrene ⁺ (C ₁₆ H ₁₀) ^b	2.6 (−18)	2.4 (−5)
Benzo(ghi)Perylene ⁺ (C ₂₂ H ₁₂) ^b	2.8 (−18)	2.2 (−5)
Coronene ⁺ (C ₂₄ H ₁₂) ^b	1.0 (−18)	6.1 (−5)
Ovalene ⁺ (C ₃₂ H ₁₄) ^c	1.2 (−18)	5.1 (−5)
Hydrogenated Amorphous Carbon solids:		
HAC/BE ^e	4.8 (−19)	1.3 (−4)
HAC/ACAR ^e	1.9 (−19)	3.2 (−4)
H5 ^f	1.9 (−19)	3.2 (−4)
H10 ^f	1.3 (−19)	4.7 (−4)
H50 ^f	2.6 (−19)	2.4 (−4)

^a Required carbon abundance to reproduce the strength interstellar 6.2 μm absorption feature

^b Hudgins & Allamandola 1995

^c Langhoff 1996

^d Schutte et al. 1993

^e Colangeli et al. 1995; abbreviations refer to HAC's prepared by different methods; BE: Burning of benzene; ACAR: Arc discharge between amorphous carbon electrodes.

^f Schnaiter et al. 1998; solid carbon prepared by condensation of carbon vapor in Ar/H₂ atmosphere. Numbers refer to % of hydrogen in quenching gas.

4.5. The 5.95 μm feature

Figs. 5 to 7 show a broad absorption structure centered at $\sim 5.95 \mu\text{m}$ (1680 cm^{-1}) next to the 6.2 μm band. A similar band was earlier seen in the spectrum of Sgr A obtained by the Kuiper Airborne Observatory (Tielens et al. 1996). This feature cannot be explained by the OH bending mode of H₂O, since the strength of the band seems to be considerably larger than that of the OH bending mode corresponding to the H₂O column density indicated by the 3 μm band, and is indeed also present for sources with no 3 μm absorption, e.g., WR104 and WR118. The position of the feature is characteristic of the stretching mode of carbonyl groups (C=O) in organic molecules. Due to the limited quality of the present data, a detailed discussion on the nature of the carbonyl groups as determined from the band profile is postponed to a later paper (Chiar et al., in prep.). In any case, the shallowness of the 5.95 μm band shows that it corresponds to at most a small quantity of oxygen (Sect. 6).

5. Gaseous vs. solid state origin of the aromatic absorbing material

The carriers of the 6.2 μm absorption feature could either be gas phase aromatic species or carbonaceous solids containing aromatic moieties. The presence of the 6.2, 7.8 and 11.2 μm emission features in the diffuse medium (Mattila et al. 1996) shows

that gaseous PAHs are widespread throughout the Galaxy and should contribute at least some small part of the 6.2 μm feature. On the other hand, to account for the interstellar UV/Visual extinction, dust models generally assume that some form of solid carbonaceous matter is an important component of interstellar dust (Li & Greenberg 1997; Mathis 1996; Schnaiter et al. 1998). This material is either aromatic from the start (e.g., graphite), or may form aromatic structures under the influence of processes in the interstellar medium (e.g., UV irradiation; Jenniskens et al. 1993; Mennella et al. 1996). In the following the gas phase and solid state origin are considered, taking into account the constraints imposed on the carrier by the strength of the 6.2 μm absorption band in terms of the required abundance, and by the profile of the feature.

5.1. Abundance constraints

The ratio of the integrated strength of the 6.2 μm absorption feature relative to the depth of the silicate band constrains the abundance of the carbonaceous carrier. For the local sources (WR118, WR112, WR104, WR98a, WR48a) the weighted average equals $\tau_{\text{int}}(6.2)/\tau(9.7) = 2.2 (\pm 0.5) \text{ cm}^{-1}$ (Table 3). This value is also consistent with the upper limit towards CygOB2 #12.

Given a band strength for the aromatic CC stretching mode, the column density and abundance of the carrier may be determined. Table 4 lists the band strength per C atom A_C for a number of aromatic materials. These are neutral PAHs, PAH cations, and some Hydrogenated Amorphous Carbon (HAC) materials prepared by a variety of methods. Furthermore, the quantity of carbon required to reproduce the absorption feature is given. This number is given by:

$$\left[\frac{N_C}{N_H} \right] = \frac{\tau_{\text{int}}(6.2)}{\tau(9.7)} \frac{1}{A_C} \left\{ \left[\frac{N_H}{A_V} \right] \left[\frac{A_V}{\tau(9.7)} \right] \right\}^{-1} \quad (2)$$

using $\tau_{\text{int}}(6.2)/\tau(9.7) = 2.2 \text{ cm}^{-1}$ (see above), $N_H/A_V = 1.9 \times 10^{21} \text{ cm}^{-2}$ (Bohlin et al. 1978), and $A_V/\tau(9.7) = 18.9$ (Roche & Aitken 1984; Whittet et al. 1997).

Table 4 shows that the strength of the 6.2 μm feature of PAHs strongly depends on the ionization state. Recent estimates of the abundance of the gaseous PAHs and PAH clusters emitting the UIR bands based on COBE data indicate $(N_C/N_H)_{\text{PAH}} = 6.1 \times 10^{-5}$ (Dwek et al. 1997). Inspection of Table 4 suggests that if the interstellar PAHs are mostly ionized, they would be able to account for the 6.2 μm absorption feature. A large ionization fraction is indeed indicated by models of the ionization equilibrium in the diffuse medium (Lepp et al. 1988; Salama et al. 1996; Dartois & d'Hendecourt 1997). Although the PAHs responsible for the 6.2 μm UIR band should be considerably larger than those listed in Table 4 (Désert et al. 1990; Schutte et al. 1993), calculations and observations indicate that the strong enhancement of the CC stretching band persists for such large ionized PAHs (Schutte et al. 1993; Langhoff 1996). We conclude that the abundance constraint can probably be well met if the 6.2 μm absorption band is attributed to gaseous PAHs and

PAH clusters similar to those responsible for the corresponding emission feature.

Table 4 shows that the strength of the 6.2 μm absorption band in bulk Hydrogenated Amorphous Carbon is comparable to that for neutral PAHs, but is considerably less than for PAH cations. Therefore, in case of a solid state carrier, this material would have to be highly abundant. For HAC/BE, which has the strongest absorption band, the amount of carbon that would be needed is $N(\text{C})/N(\text{H}) = 1.3 \times 10^{-4}$. This would still be consistent with models of interstellar dust, which use similar quantities of solid carbon (either as mantles on silicate grains, or as separate particles) to model the interstellar extinction curve (Li & Greenberg 1997; Mathis 1996; Schnaiter et al. 1998). It is however somewhat higher than the “cosmic abundance” constraint which limit the amount of carbon in dust and PAHs combined to $\sim 8 \times 10^{-5}$ (Cardelli et al. 1996; Snow & Witt 1996; Sofia et al. 1997). It must be noted though that some doubt remains whether the “cosmic abundance”, which is obtained indirectly from observations of O and B stars, is truly representative of the interstellar medium (Tielens et al. 1996; Schnaiter et al. 1998). Using the other forms of solid carbon in Table 4 to account for the 6.2 μm feature clearly exceeds the abundance constraints set by both the results of grain models and by the cosmic abundance. We conclude that, although the amount of carbon locked up in carbon dust is probably larger than in PAHs, the considerably smaller strength of the CC stretching mode makes it harder to satisfy the abundance constraint with bulk aromatic matter than with ionized gaseous PAHs.

5.2. Spectroscopic constraints

While the interstellar absorption and emission bands correspond well in position and width, the observed 6.2 μm absorption band and the feature of anthracite coal are clearly different. The anthracite band is shifted redward by about 20 cm^{-1} , and is much broader than the interstellar feature (60 vs 35 cm^{-1}). Different kinds of hydrogenated amorphous carbon prepared in the laboratory by a variety of techniques (laser ablation of graphite in a hydrogen atmosphere, burning of hydrocarbons, arc discharge between carbon electrodes, plasma deposition from a discharge in benzene vapor) show similar discrepancies (Borghesi et al. 1987; Scott & Duley 1996; Scott et al. 1997; Colangeli et al. 1995; Dischler et al. 1983; Schnaiter et al. 1998). The large width of the solid state feature is caused by interactions between molecular (sub-)groups in the inhomogeneous environment of the amorphous carbon matrix. It thus seems that the spectral properties of the 6.2 μm absorption band are hard to reconcile with an origin in bulk carbonaceous matter.

5.3. Discussion

The spectroscopic constraints show that the carrier of the 6.2 μm feature has properties similar to gaseous aromatic species, but unlike that of bulk carbonaceous matter. This would limit the size of the carriers to particles containing at most a few thousand C atoms. This would imply that the carriers of the absorption

feature fall in the same size range as the carriers of the UIR emission bands (Schutte et al. 1993). It was argued in Sect. 5.1 that the abundance constraints also appear to be consistent with such an origin. We conclude that the 6.2 μm absorption band, like the corresponding emission band, probably originates in gaseous PAHs and PAH clusters of size up to a few thousand C atoms.

6. Composition of the carbonaceous grain component

The absence of strong features in the spectra of our sources (Fig. 2) shows that the carbonaceous dust material in the diffuse medium is only weakly infrared active. This is significant, because vibrational modes of subgroups in organic solids produce a number of strong features in the mid infrared. Of these only the aliphatic CH stretching and (weakly) carboxyl CO stretching features are observed. Upper limits for a number of other infrared modes are listed in Table 5. We choose to list the values towards WR118, since its high column density and absence of solid H_2O makes this object the most sensitive probe for organic features. Also an upper limit to the abundance of the organic groups in the carbon dust is given, $N/N_{\text{solid}}(\text{C})$, assuming a solid carbon abundance of 1.5×10^{-4} relative to H (Mathis 1996; Li & Greenberg 1997).

Table 5 shows that about 13% of the carbon atoms in the carbonaceous solids in the local ISM have an aliphatic character. Similar abundances were earlier derived from ground based observation of the 3.4 μm absorption towards the galactic center and local sources suffering from diffuse medium extinction (Wickramasinghe & Allen 1980; Sandford et al. 1991; Pendleton et al. 1994). The quantity of aromatic CH bonds is constrained to less than 18% of the solid carbon. Thus the hydrogen content of the carbonaceous dust material lies in the range $0.13 \lesssim \text{H/C} \lesssim 0.31$.

There is no indication of the strong OH stretching mode of organic hydroxy groups near 3 μm . Although the carbonyl (C=O) 6 μm feature is likely present towards our sources (Sect. 4), the corresponding amount of oxygen is low (Table 5). Together with the upper limit to hydroxy (-OH) groups, this results shows that the abundance of oxygen in the carbonaceous material in the diffuse line of sight towards WR118 equals $\text{O/C} \lesssim 0.11$.

Table 5 also lists upper limits to the abundance of some nitrogen-containing organic groups. A stringent upper limit is found for nitriles.

A detection of the 3.3 μm aromatic stretching mode in absorption was reported by Sellgren et al. (1995) towards the embedded protostellar source MonR2/IRS3. The corresponding quantity of aromatic CH groups was $N/N(\text{H}) = 1.3 \times 10^{-5}$, well below the upper limit towards WR118 (Table 5). Scaled to the H column density for our sources, the expected optical depth of the 3.3 μm feature is 0.005 - 0.01, a factor 2 to 4 below the detection limits. A prior detection of the 6.2 μm feature in absorption towards the high mass young stellar object NGC7538:IRS9 was reported by Schutte et al. (1996). The strength of this band per unit silicate depth is somewhat lower than for the 6.2 μm feature

Table 5. (Upper limits to) the integrated strengths of features of several organic molecular groups as observed towards WR118, with corresponding abundances. The hydrogen column density towards this source, derived from the depth of the 9.7 μm feature, equals $2.5 \times 10^{22} \text{ cm}^{-2}$

Feature	Position		FWHM		Band strength ^a cm/C atom	τ_{int} cm ⁻¹	N/N(H)	N/N _{solid} (C)
	cm ⁻¹	μm	cm ⁻¹	μm				
R – NH ₂ ; NH str.	3380 ^b	2.96	170 ^b	0.15	1.7 (–18)	<6	<1.4 (–4)	< 0.93
Hydroxy OH stretch	3290 ^b	3.04	300 ^b	0.28	5 (–17)	<17	<1.3 (–5)	< 0.09
Aromatic CH stretch	3040	3.29	40	0.04	1.3 (–18) ^d	<0.9	<2.7 (–5)	< 0.18
Combined aliphatic asym. CH ₂ /CH ₃ stretch	2920	3.42	65	0.08	7 (–18) ^c	3.4	1.9 (–5)	0.13
Nitrile CN str.	2248 ^b	4.45	20 ^b	0.04	1 (–17) ^e	< 0.6	<2.4 (–6)	< 0.016
Carbonyl CO stretch	1710 ^b	5.85	40 ^b	0.14	2 (–17)	1.6	3.2(–6)	0.021
Aromatic CC stretch	1610	6.21	38	0.15	–	2.3	–	–
Hexamethylene Tetramine ^f	1000	10.0	18	0.18	8.3 (–19)	< 1.1	< 5.2 (–5)	< 0.34
Aromatic CH bend	890	11.24	22	0.28	3.2 (–18) ^d	<1.0	<1.2 (–5)	< 0.08

^a Wexler 1967, unless otherwise noted; ^b Aldrich 1981; ^c Averaged over the CH₂ and CH₃ contributions (Tielens et al. 1996);

^d Schutte et al. 1993; ^e Bernstein et al. 1997; ^f Bernstein et al. 1995

in the diffuse sources of this paper. However, baseline ambiguities make the shape and strength of this band uncertain, and we therefore postpone a detailed discussion to a later paper (Keane et al., in preparation).

An upper limit to the abundance of Hexamethylene Tetramine (HMT) is also provided by Table 5. HMT is the dominant product in the organic material produced by the photolysis of ices containing considerable quantities of methanol (Bernstein et al. 1995), and could be present if UV processing of ices in dense interstellar clouds is the origin of the carbonaceous mantles (Greenberg 1979; Greenberg et al. 1995; see also Sect. 7).

7. Discussion

The 6.2 μm absorption feature in the diffuse medium is the absorption counterpart of the well-known UIR emission band at this wavelength. Its strength is consistent with current best estimates of the abundance of carbon in gaseous PAHs of $\sim 6 \times 10^{-5}$ relative to hydrogen, showing that the interstellar PAH abundance cannot be much lower than this. Furthermore, it indicates that the strong enhancement of the 6.2 μm feature upon ionization observed for PAHs up to ~ 30 C atoms (Langhoff 1996) should also occur for the few hundred C atom PAHs which contribute most of the absorption feature. This conclusion was earlier reached from modelling of the UIR emission spectrum (Schutte et al. 1993).

There appears to be no significant difference in the strength of the 6.2 μm band per unit silicate band depth for the Galactic Center Sources and the more local sources (Table 3). A decrease of the abundance of PAHs would be expected if they are primarily formed in the outflow of Carbon-rich mass losing AGB stars (Frenklach & Feigelson 1989; Cherchneff et al. 1993), since the number of Carbon- relative to Oxygen-rich AGB stars drops considerably towards the Galactic Center (Blanco 1965; Thronson et al. 1987; Jura 1990). The constancy of the strength of the 6.2 μm band towards the GC may thus indicate that con-

densation in the outflow of Carbon stars is not the main source of interstellar PAHs.

The absence or weakness of features due to organic molecular groups besides the well-known 3.4 μm aliphatic CH stretching band shows that interstellar carbonaceous dust material is poor in oxygen as well as hydrogen. An extensive discussion of the possible ways of forming interstellar dust was given by Tielens et al. (1996). Basically, two different sources of carbonaceous dust may be considered. First, carbon particles can be injected into the ISM by Carbon-rich AGB stars as well as other mass-losing objects such as supernovae. Second, carbonaceous dust may be formed in-situ in the ISM, likely through energetic processing of the icy mantles on grains inside dense clouds (Greenberg 1979; Greenberg et al. 1995). In the former case the low oxygen content is readily explained by the formation of CO in the stellar outflow, which consumes the oxygen prior to the formation of the carbon grains (Cherchneff 1997). The low hydrogen content is explained by the high condensation temperature for the carbon particles in the stellar outflow (~ 1000 K; Martin & Rogers 1987), preventing the incorporation of hydrogen in the solid (Borghesi et al. 1987; Mortera & Low 1983). On the other hand, UV photolysis of interstellar ice analogs containing H₂O and CO result in organic material that is highly oxygen and hydrogen rich (Agarwal et al. 1985; Briggs et al. 1992). Therefore, if production took place by processing of such ices, the original organic material must have been thoroughly carbonized by, e.g. UV irradiation in the diffuse interstellar medium (Jenniskens et al. 1993). While such processing should lead to a steady decrease of the oxygen content, the dehydrogenation may be balanced by reactions with the abundant hydrogen atomic gas. Thus the degree of hydrogenation of the solid carbon in the diffuse medium could be the result of the equilibrium between these processes, rather than reflect the composition of the material at its formation. Further laboratory work is necessary to investigate this possibility. If methanol was the dominant carbon carrier in the original dense cloud ices, the organic material produced by UV irradiation is oxygen poor

and is dominated by the formaldehyde polymerization product Hexamethylene Tetramine ($\text{C}_6\text{H}_{12}\text{N}_4$; Bernstein et al. 1995). The upper limit to the quantity of HMT in the interstellar solid carbon is presently not very strict (Table 5). Further observational and experimental studies are necessary to test whether the observational constraints to the composition of the carbonaceous grain material can be reproduced by processing in the diffuse medium of organic material created by irradiation of icy mantles in dense clouds.

8. Conclusions

Spectroscopy of Galactic Center sources GCS 3 and GCS 4 and of a number of local infrared sources obscured by diffuse medium dust reveals interstellar absorption bands at 3.0, 3.4, 4.27, 4.66, 5.95 and 6.2 μm . The 4.27 and 4.66 μm features are ascribed to solid CO_2 and gaseous CO which indicate the presence of dense cloud extinction towards some of our sources. While the 3.0 μm band appears to grow together with these features, the 3.4, 5.95 and 6.2 μm band do not show any correlation. Indeed some sources show these latter bands exclusively with no trace of the other features. We thus conclude that the 3.0 μm feature probably originates in dense cloud extinction and should be primarily due to H_2O ice. The depth of the feature indicates that the fraction of non-translucent dense material in the line-of-sight is less than $\sim 10\%$ for all objects. The 3.4, 5.95 and 6.2 μm features can be ascribed to components of the diffuse medium. The 3.4 μm feature was observed previously and is identified with the CH stretching modes of CH_2 and CH_3 groups in aliphatic solids. The 5.95 μm feature which was observed previously by air-borne spectroscopy, is ascribed to carbonyl groups in solid carbonaceous material. The 6.2 μm band is first observed by ISO. An assignment to the OH bending mode of solid H_2O , either icy or as “water of hydration” inside the silicates, can be excluded due a poor spectral correspondence and the absence of the corresponding OH stretching feature. The 6.2 μm feature is very similar in position and width to the well-known interstellar emission feature, pointing to an origin in aromatic materials.

The limited width as well as the position of the 6.2 μm absorption seems inconsistent with an origin in bulk carbonaceous matter. The good correspondence with the interstellar emission feature indicates that it originates in the CC stretching mode of gaseous PAHs and PAH clusters similar to those responsible for the emission bands. The absence of bulk properties limits the size of the contributing clusters to less than a few thousand carbon atoms. The strength of the band is consistent with current best estimates of the interstellar PAH abundance and the strength of the CC stretching mode of ionized PAHs. The absence of additional PAH features in the present data is consistent with such a carrier, although models predict that the 3.3 and 11.2 μm absorption features should become apparent when the present S/N noise level is improved by a factor 2-4.

No significant difference was found in the ratio of the 6.2 μm absorption to the 9.7 μm silicate band when comparing the local and the galactic center sources. This indicates that there is

little or no gradient in the abundance of PAHs and PAH clusters towards the galactic center.

The non-detection of the strong stretching modes of the hydroxyl (OH) and carbonyl (CO) organic groups in any of our lines-of-sight indicates that the carbonaceous dust material in the diffuse interstellar medium probably contains only small quantities of oxygen ($\text{O}/\text{C} \lesssim 0.11$). Likewise the amount of hydrogen is limited ($0.13 \lesssim \text{H}/\text{C} \lesssim 0.31$). This indicates that the carbon dust either originates from carbon stars, or was formed from the oxygen and hydrogen rich organic material produced by energetic processing of ices in dense clouds, by subsequent heavy UV processing in the diffuse medium.

Acknowledgements. We would like to thank Douwe Beintema for supplying the electronic version of the SWS spectrum of NGC7027. We also mention scientific support by Harm Habing on the issue of the galactic distribution of Carbon and Oxygen-rich AGB stars. Comments by the anonymous referee substantially improved the paper. This work was partially funded by NASA grant NGR 33-018-148 and by an ASTRON grant from the Netherlands Organization for Scientific Research (NWO). Support for W. S. from SRON is acknowledged as well. D. C. B. W. is funded by NASA grants NAGW-3144 and NAGW-4039.

References

- Agarwal V.K., Schutte W., Greenberg J.M., Ferris J.P., Briggs R., Connor S., van de Bult C.P.E.M., Baas F. 1985, *Origins of Life* 16, 21
- Aldrich Library of Infrared Spectra ed. III 1981, ed. C.J. Pouchert. Milwaukee, Aldrich
- Allamandola L.J., Tielens A.G.G.M., Barker J.R. 1985, *ApJ* 290, L25
- Allamandola L.J., Tielens A.G.G.M., Barker J.R. 1989, *ApJS* 71, 733
- Beintema D.A., van den Ancker M.E., Molster F.J., et al. 1996, *A&A* 315, L369
- Bernstein M.P., Sandford S.A., Allamandola L.J., Chang S., Scharberg M.A. 1995, *ApJ* 454, 327
- Bernstein M.P., Sandford S.A., Allamandola L.J. 1997, *ApJ* 476, 932
- Blanco, V. M. 1965, in: *Galactic Structure*, M. Blaauw and M. Schmidt (eds.). University of Chicago press, Chicago p. 241
- Bohlin R.C., Savage B.D., Drake J.F. 1978, *ApJ* 224, 132
- Borghesi A., Bussoletti E., Colangeli L. 1987, *ApJ* 314, 422
- Bregman J.D., Allamandola L.J., Tielens A.G.G.M., Geballe T.R., Witteborn F.C. 1989, *ApJ* 344, 791
- Briggs R., Ertem G., Ferris J.P., et al. 1992, *Origins of Life and Evolution of the Biosphere* 22, 287
- Butchart I., McFadzean A.D., Whittet D.C.B., Geballe T.R., Greenberg J.M. 1986, *A&A* 154, L5
- Cardelli J.A., Meyer D.M., Jura M., Savage B.D. 1996, *ApJ* 467, 334
- Cherchneff I. 1997, in: *Molecules in astrophysics; Probes and processes*, Proc. IAU Symp. 178, ed. E. F. van Dishoeck, Kluwer, Dordrecht, p. 469
- Cherchneff I., Barker J.R., Tielens A.G.G.M. 1993, *ApJ* 413, 445
- Chiar J.E., Adamson A.J., Kerr T.H., Whittet D.C.B. 1995, *ApJ* 455, 234
- Cohen M., Allamandola L.J., Tielens A.G.G.M., et al. 1986, *ApJ* 302, 737
- Cohen M., Tielens A.G.G.M., Bregman J.D. 1989, *ApJ* 344, L13
- Colangeli L., Mennella V., Palumbo, P., Rotundi A., Bussoletti E. 1995, *A&AS* 113, 561
- Cook D.J., Saykally R.J. 1998, *ApJ* 493, 793

- Dartois E., d'Hendecourt L. 1997, *A&A* 323, 534
- de Graauw Th., Haser L.N., Beintema D.A., et al. 1996a, *A&A* 315, L49
- de Graauw Th., Whittet D.C.B., Gerakines P.A., et al. 1996b, *A&A* 315, L345
- Désert F.-X., Boulanger F., Puget J.L. 1990, *A&A* 237, 215
- Dischler B., Bubbenzer A., Koidl P. 1983, *Solid State Comm.* 48, 105
- d'Hendecourt L.B., Allamandola L.J. 1986, *A&AS* 64, 453
- Draine B.T. 1989, in: *IAU symposium 135, Interstellar Dust*, eds. L.J. Allamandola and A.G.G.M. Tielens, Kluwer, p. 313
- Dwek E., Arendt R.G., Fixsen D.J., et al. 1997, *ApJ* 475, 565
- Frenklach M., Feigelson E.D. 1989, *ApJ* 341, 372
- Gillett F.C., Jones T.W., Merrill K.M., Stein W.A. 1975, *A&A* 45, 77
- Greenberg J.M. 1974, *ApJ* 189, L81
- Greenberg J.M. 1979, in: *Stars and Starsystems*, ed. B. E. Westerlund. Reidel, Dordrecht, p. 173
- Greenberg J.M., Li A., Mendoza-Gómez C.X., Schutte W.A., Gerakines P.A., de Groot M. 1995, *ApJ* 455, L177
- Guillois O., Nenner I., Papoular R., Reynaud C. 1996, *ApJ* 464, 810
- Gürtler J., Henning T., Kömpe C., et al. 1996, *A&A* 315, L189
- Hudgins D.M., Allamandola L.J. 1995, *J. Phys. Chem.* 99, 3033
- Humphreys R.M. 1978, *ApJS* 38, 309
- Imanishi M., Sasaki Y., Goto M., et al. 1996, *AJ* 112, 235
- Jenniskens P., Baratta G. A., Kouchi A. et al. 1993, *A&A* 273, 583
- Joblin C., Boissel P., Léger A., d'Hendecourt L., Défourneau D. 1995, *A&A* 299, 835
- Jones A.P., Tielens A.G.G.M., Hollenbach D.J., McKee C.F. 1994, *ApJ* 433, 797
- Jones A.P., Tielens A.G.G.M., Hollenbach D.J. 1996, *ApJ* 469, 740
- Jura M. 1987, in: *Interstellar processes*, eds. D.J. Hollenbach and H.A. Thronson, Reidel, Dordrecht, p. 3
- Jura M. 1990, in: *From Mira's to Planetary nebulae: Which Path for Stellar Evolution?*, M. O. Mennessier and A. Omont (eds). Editions Frontières, Singapore, p. 41.
- Kessler M.F., Steinz J.A., Anderegg M.E., et al. 1996, *A&A* 315, L27
- Kim S., Martin P.G., Hendry P.D. 1994, *ApJ* 422, 164
- Lacy J.H., Baas F., Allamandola L.J., et al. 1984, *ApJ* 276, 533
- Langhoff S.R. 1996, *J. Phys. Chem.* 100, 2819
- Léger A., Puget J.-L. 1984, *A&A* 137, L5
- Leitherer C., Bertout C., Stahl O., Wolf O. 1984, *A&A* 140, 199
- Lepp S., Dalgarno A., van Dishoeck E.F., Black J.H. 1988, *ApJ* 329, 418
- Li A., Greenberg J.M. 1997, *A&A*, in press
- Lutz D., Feuchtgruber H., Genzel R., et al. 1996, *A&A* 315, L269
- Martin P.G., Rogers C. 1987, *ApJ* 322, 374
- Mathis J.S. 1996, *ApJ* 472, 643
- Mathis J., Mezger P., Panagia N. 1983, *A&A* 128, 212
- Mattila K., Lemke D., Haikala L.K., et al. 1996, *A&A* 315, L353
- McFadzean A.D., Whittet D.C.B., Longmore A.J., Bode M.F., Adamson A.J. 1989, *MNRAS* 241, 873
- Mennella V., Colangeli L., Palumbo P., et al. 1996, *ApJ* 464, L191
- Meyer D.M. 1997, in: *Molecules in Astrophysics: Probes and Processes*, ed. E.F. van Dishoeck. Kluwer, Dordrecht, p. 407
- Mortera C., Low M.J.D. 1983, *Carbon* 2, 283
- Nagata T., Woodward C.E., Shure M., Pipher J.L., Okuda H. 1990, *ApJ* 351, 83
- Nuth III, J. A. 1996, in: *The cosmic dust connection*, J. M. Greenberg (ed.) Kluwer academic publishers, Dordrecht, p. 205
- Onaka T., Yamamura I., Tanabé T., Roellig T.L., Yuen L. 1996, *PASJ* 48, L59
- Okuda H., Shibai H., Nakagawa T., et al. 1990, *ApJ* 351, 89
- Pendleton Y.J., Sandford S.A., Allamandola L.J., Tielens A.G.G.M., Sellgren K. 1994, *ApJ* 437, 683
- Persi P., Ferrari-Tonioli M. 1982, *A&A* 111, L7
- Ristorcelli I., Giard M., Mény C., et al. 1994, *A&A* 286, L23
- Roche P.F., Aitken D.K. 1984, *MNRAS* 208, 481
- Roche P.F., Aitken D.K. 1985, *MNRAS* 215, 425
- Russell R.W., Soifer B.T., Willner S.P. 1977, *ApJ* 217, L149
- Salama F., Allamandola L.J. 1993, *J. Chem. Soc. Faraday Trans.* 89, 2277
- Salama F., Bakes E., Allamandola L.J., Tielens A.G.G.M. 1996, *ApJ* 458, 621
- Sandford S.A., Allamandola L.J., Tielens A.G.G.M., et al. 1991, *ApJ* 371, 607
- Schnaiter M., Mutschke H., Dorschner J., Henning Th., Salama F. 1998, *ApJ*, in press
- Schutte W.A. 1988, PhD thesis, University of Leiden, Leiden
- Schutte W., Greenberg J. M. 1986, in: *Light on Dark Matter*, ed. F. P. Israel. Reidel, Dordrecht, p. 229
- Schutte W., Greenberg J. M. 1988, in: *Dust in the Universe*, M. E. Bailey and D. A. Williams (eds.). Cambridge University press, Cambridge, p. 403
- Schutte W.A., Tielens A.G.G.M., Allamandola L.J. 1993, *ApJ* 415, 397
- Schutte W.A., Tielens A.G.G.M., Whittet D.C.B., et al. 1996 *A&A* 315, L333
- Sellgren K., Brooke T.Y., Smith, R.G., Geballe T.R. 1995, *ApJ* 449, L69
- Scott A.D., Duley W.W. 1996, *ApJ* 472, L123
- Scott A.D., Duley W.W., Jahani H.R. 1997, *ApJ* 490, L175
- Snow T.P., Witt A.N. 1996, *ApJ* 468, L6
- Sofia U.J., Cardelli J.A., Guerin K.P., Meyer D.M. 1997, *ApJ* 482, L105
- Spitzer L. 1978, *Physical Processes in the Interstellar Medium*, Wiley, New York
- Thronson H.A., Latter, W.B., Black J.H., Bally J., Hacking P. 1987, *ApJ* 322, 770
- Tielens A.G.G.M., Tokunaga A.T., Geballe T.R., Baas F. 1991, *ApJ* 381, 181
- Tielens A.G.G.M., Wooden D.H., Allamandola, L.J., Bregman, J., Witteborn F.C. 1996, *ApJ* 461, 210
- van der Hucht K.A. 1992, *A&A Review* 4, 123
- van der Hucht K.A., Morris P.W., Williams P.M., et al. 1996, *A&A* 315, L193
- van Dishoeck E.F., Black J.H. 1986, *ApJS* 62, 109
- van Dishoeck E.F., Helmich F.P., de Graauw Th., et al. 1996, *A&A* 315, L349
- Wada S., Sakata A., Tokunaga A.T. 1991, *ApJ* 375, L17
- Wexler A.S. 1967, *Applied Spectroscopy Review* 1, 29
- Whittet D.C.B., Bode M.F., Longmore A.J., et al. 1988, *MNRAS* 233, 321
- Whittet D.C.B., Schutte W.A., Tielens A.G.G.M., et al. 1996, *A&A* 315, 357
- Whittet D.C.B., Boogert A.C.A., Gerakines P.A., et al. 1997, *ApJ* 490, 729
- Wickramasinghe D.T., Allen D.A. 1980, *Nat* 287, 518
- Williams P.M. 1995, in: *Wolf-Rayet stars: Binaries, Colliding Winds, Evolution*, Proc. IAU Symp. 163, K. A. van der Hucht & P. M. Williams (eds.). Kluwer, Dordrecht, p. 335
- Willner B.T., Soifer R.W., Russell R.W., Joyce R.R., Gillett F.C. 1977, *ApJ* 217, L121